International Journal of Thermal Sciences 200 (2024) 108946

Contents lists available at ScienceDirect

International Journal of Thermal Sciences

journal homepage: www.elsevier.com/locate/ijts

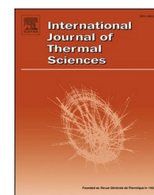

A transient thermal model for forecasting the real-time temperature of downhole electronics

Fulong Wei [a], Wei Lan [b], Chao Deng [b], Jiale Peng [b], Xiaobing Luo [a,b,*]

[a] School of Physics, Huazhong University of Science and Technology, Wuhan, China
[b] School of Energy and Power Engineering, Huazhong University of Science and Technology, Wuhan, China

ARTICLE INFO

Keywords:
Logging tool
Downhole electronics
High-temperature environment
Passive thermal management
Temperature prediction

ABSTRACT

Logging tools are essential for high-temperature downhole oil exploration. Passive thermal management has been widely used to ensure the normal operation of downhole electronics. A key requirement for passive thermal management is the quick on-site prediction of real-time logging tool temperature. This is challenging due to variable downhole environments, initial temperature distributions, and power dissipations of heat sources. To address this issue, a transient thermal model for predicting the real-time temperature of logging tools is proposed. This model is based on a thermal network model with a discrete thermal equilibrium equation and considers heat transfer processes inside and outside the logging tool. The proposed model considers both the accuracy and the efficiency of prediction and can be applied under different working conditions. The average relative error between the proposed model and the experiment is only 6.5 %. In addition, the computing time and resources of the proposed model are significantly reduced compared with traditional numerical simulations. The proposed prediction model shows promise for wide use in real-time logging tool operations.

1. Introduction

With the growing demand for oil and gas resources worldwide, petroleum exploration has gradually focused on deeper wells due to the depletion of shallow and medium-depth oil fields [1]. The downhole ambient temperature increases with well depth, and the temperature of wells can exceed 200 °C [2,3]. Logging tools, as key equipment for measuring the physical and chemical properties of rock formations, are widely used for exploring downhole oil and gas resources [4]. Compared with other logging tool components, internal electronics such as integrated circuits are the most susceptible to failure due to the high-temperature environment [5]. Therefore, effective thermal management measures need to be adopted to protect the normal operation of electronics inside a logging tool.

Currently, thermal management measures can be divided into active cooling systems (ACSs) and passive thermal management systems (PTMSs). ACSs mainly include vapor compression refrigeration [6–8], Stirling cooling [9,10], adsorption cooling [11,12] and thermoelectric cooling [13–15]. ACSs have the advantage of long-term temperature control performance [16]. However, due to the existence of moving parts, complex structures, and external energy inputs, the reliability of these systems is too low to be widely applied to actual operations [17,18]. Compared to ACSs, PTMSs possess the highest reliability and are more prevalent in logging applications [19,20]. Fig. 1 shows a schematic diagram of a typical PTMS. A vacuum flask combined with insulators is utilized to insulate the heat intrusion from the ambient environment. Phase change heat sinks are applied to absorb the heat generated from the electronics and intruded from the high-temperature environment. During operation, the temperature of the electronics inside the tool climbs constantly due to the accumulation of heat. However, electronics can only withstand a certain temperatures range. Hence, PTMSs can only protect electronics for a limited number of hours [21]. It is necessary to keep track of the remaining safe operating time (RSOT) of the tool in real time. The RSOT represents the period from the current to the threshold temperature of electronics, which requires temperature prediction as input. Therefore, the RSOT of a tool in a high-temperature well depends on many parameters, such as the ambient temperature, initial temperature distribution of the tool, and heat dissipation of the electronics. As an input condition, accurately and quickly predicting the temperature of the instrument under different operating conditions is particularly important.

Current methods for the temperature prediction of electronic devices are mainly based on two principles: data-driven and heat transfer

* Corresponding author. School of Physics, Huazhong University of Science and Technology, Wuhan, China.
E-mail address: luoxb@hust.edu.cn (X. Luo).

https://doi.org/10.1016/j.ijthermalsci.2024.108946
Received 29 November 2023; Received in revised form 22 January 2024; Accepted 29 January 2024
Available online 6 February 2024
1290-0729/© 2024 Elsevier Masson SAS. All rights reserved.

Nomenclature

ρ	Density kg/m^3
c	Specific heat capacity kJ/(kg·K)
V	Volume m^3
λ	Thermal conductivity W/(m·K)
Q	Self-generating heat W
R	Thermal resistance K/W
Δt	Time step s
T	Temperature K
l	Length of each node m
S	Effective heat exchange area m^2
r	Radius m
L	Latent heat kJ/kg
h	Convection heat transfer coefficient $W/(m^2 \cdot K)$
T_s	Initial phase change temperature of PCM K
T_l	Final phase change temperature of PCM K
c_{eff}	Equivalent heat capacity of PCM kJ/(kg·K)
T_{out}	Temperature of downhole environment K
r^{in}	Inner radius of the cylindrical node m
r^{out}	Outer radius of the cylindrical node m

Subscripts

m	Quantity of neighbor nodes involved in heat exchange
i	Node i
j	Neighbor node j
s	Solid PCM
l	Liquid PCM
t	Moment

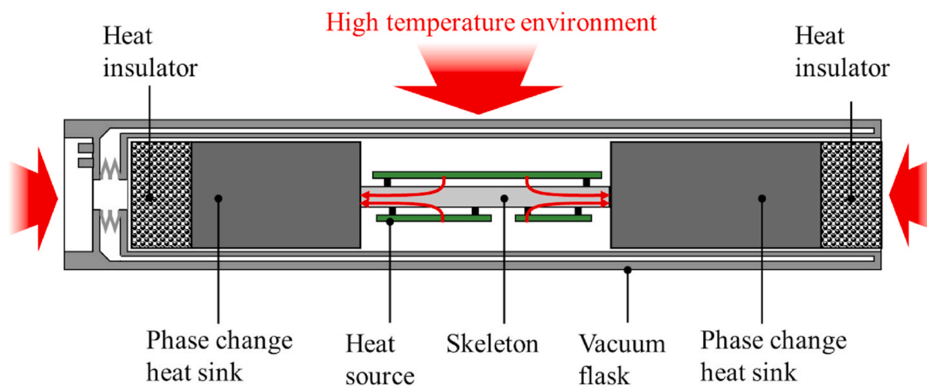

Fig. 1. Schematic diagram of a typical downhole PTMS.

models. Because they are limited by dataset size, data-driven models have difficulty obtaining complete temperature data to cover all working conditions [22,23]. Some of them rely on historical data, and thus the predictable temperature duration is limited to 60 min [24,25]. Therefore, data-driven models are not suitable for predicting temperatures under varied working conditions.

In contrast, the physical mechanism of heat transfer models is clear, and no actual measurement data are needed. All operating conditions can be covered, and prediction accuracy can be guaranteed. With the development of numerical simulation techniques, the currently available 3D models have become gradually able to fully resolve complex heat transfer processes such as heat conduction, convection, and radiation inside a logging tool. Lan et al. proposed a thermal model for a downhole DTMS without considering convection and radiation inside [26]. The maximum relative error between this model and the experimental results was lower than 10 %. Based on Lan's work, Peng et al. improved model accuracy by integrating various heat transfer processes within the tool [27]. Their proposed model could accurately characterize the real heat transfer process with a deviation of 4.71 % from the experiment. However, their processes could not be integrated into embedded devices for rapid temperature prediction on-site because of the long calculation time and massive computing resource requirements. Therefore, a dimension-reduction model must be integrated into the downhole device. Current one-dimensional heat transfer models for logging tools are mainly applied to the steady-state heat transfer process [28,29]. There is no accurate model for a complex structure that includes a transient phase change process. Therefore, previous models are not applicable for predicting the remaining working time of a tool in real time. To avoid the risk of electronic failure, there is an urgent need to devise a model for accurately and efficiently predicting the temperature. First, this model must be applicable under variable operating conditions and achieve certain accuracy; second, it should be integrated into embedded equipment for predicting real-time temperature with a calculation time of no more than 1 s; and finally, it should ensure a certain length of prediction.

In this paper, a transient thermal model for logging tools was

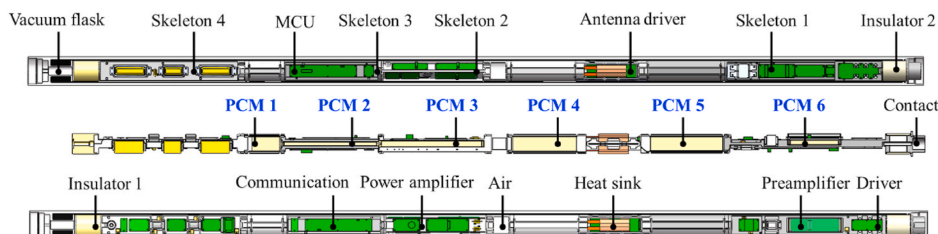

Fig. 2. Diagram of an actual PTMS of a logging tool [26].

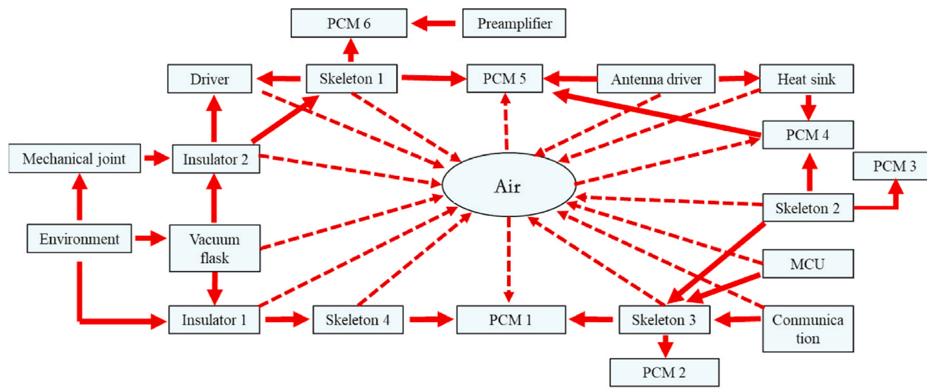

Fig. 3. Heat transfer network of the discrete nodes of the logging tool.

proposed. The logging tool was discretized into multiple thermal nodes, and a thermal network model between nodes was constructed and solved. The prediction results of the model were verified by comparison with those of the experiment and 3D numerical simulations to check the accuracy and efficiency.

2. Model

2.1. Geometry

Fig. 2 shows a diagram of the overall structure of the PTMS. During operation, the whole skeleton is loaded inside a vacuum flask. A vacuum layer between the inner and outer walls of the flask is utilized to isolate the heat leakage from the high-temperature environment. Specifically, the interlayer of the vacuum layer is evacuated to reduce the heat conduction and convection heat transfer. Within the vacuum layer, multiple layers of highly reflective screens are inserted to decrease the radiation heat transfer. To prevent the thermal conduction caused by the contact between reflective screens, low thermal conductivity fillers such as glass fibers are inserted between each pair of reflective screens. In addition, two thermal insulators are placed at the left and right ends of the system to isolate axial heat leakage. There are a total of 14 circuit boards bolted to the metal skeleton, which are thermally connected to the skeleton by thermal interface material (TIM). Their self-generating heat is absorbed by the skeleton and phase change materials (PCMs) between and inside the skeleton. The PCMs are divided into 6 heat storage modules, which are distributed in various locations of the skeleton to minimize the total heat transfer distance between heat sources and PCMs. Eventually, the thermal resistance from electronics to the heat sink is reduced.

2.2. Discretization and heat transfer network analysis

Logging tools face complex heat transfer processes during high-temperature downhole operations, including convection heat transfer between the downhole fluid and the vacuum flask, high vacuum multilayer adiabatic, phase change heat storage, heat conduction, natural air convection, and thermal radiation inside the flask. Therefore, the heat transfer process needs to be simplified to balance the accuracy and efficiency of the calculation. Several assumptions are presented as follows.

(a) The heat transfer process between the components of the tool is assumed to be transient heat transfer between a finite number of nodes.
(b) Due to the low power consumption and the high thermal uniformity, the internal thermal resistance or the temperature difference inside each node is neglected.
(c) Transient heat transfer during a single time step is equal to a quasi-static process [30,31].
(d) The vacuum layer of the flask is assumed to be a solid zone with low thermal conductivity.

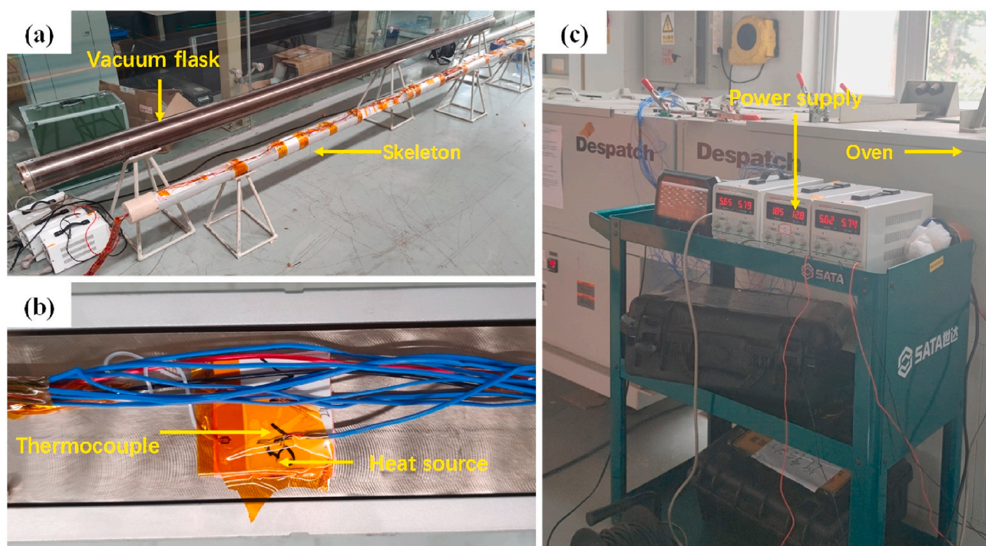

Fig. 4. High-temperature experimental setup: (a) prototype of the logging tool; (b) ceramic heating pads and thermocouple; (c) overall experimental setup.

Table 1
Materials and thermal properties of components inside the logging tool.

Name		Material	Thermal conductivity ($W\cdot m^{-1}\cdot K^{-1}$)	Density ($kg\bullet m^{-3}$)	Specific heat capacity ($J\bullet kg^{-1}\bullet K^{-1}$)
Vacuum bottle		TC-11	7.5	4480	550
Vacuum layer [33]		Aluminum foil + spacers	0.0002	100	1200
Skeleton		Aluminum alloy	130	2810	960
Heat source		Ceramics	20	2145	750
PCMs	shell	Aluminum alloy	130	2810	960
	filler	Paraffinic	0.2	880(s)/ 770(l)	Eq. (7)
Insulator	shell	PEEK	0.25	2200	1000
	filler	Aerogel	0.018	200	502.3
Heat sink		Copper	400	8700	385
Mechanical joint		Titanium alloy	7.5	4940	710

(e) The equivalent heat capacity method is utilized to describe the phase change heat storage process [32].
(f) The radiation inside the flask is ignored due to its small effect on the actual temperature [26].

Fig. 3 shows that the logging tool is decomposed into 21 nodes based on the location and function of each part. The vacuum flask, thermal insulators, PCMs, five major skeletons, and circuit boards (MCU, communication and antenna driver, etc.) are included in the main nodes. Note that these nodes consist of one component or multiple parts with different materials and heat dissipation. For example, Table 1 shows that the PEEK shells and aerogel are treated as one node. Therefore, the thermal properties of these nodes are determined by the weighted volume of all components. The self-generating heat of these nodes is defined as the total heat dissipation of all parts inside the node. Besides, the values of the initial phase change temperature of PCM(T_s) and the final phase change temperature of PCM(T_l) significantly affect the temperature of PCMs. The values of T_s and T_l are determined as 70.84 °C and 73.73 °C according to the DSC tests.

The network in Fig. 3 indicates that heat transfer only occurs between nodes in direct contact. The sources of heat are high-temperature environments and electronic devices. Specifically, the heat from the downhole environment penetrates the interior of the logging tool through the vacuum flask and insulators and then affects the temperature of each node inside. The self-generating heat of the electronics is emitted toward neighboring nodes and is continuously absorbed by the skeleton and PCMs. The air inside the vacuum flask remains in direct contact with most nodes, and as a result, the heat flow is distributed, and the overall temperature uniformity is enhanced. Nevertheless, because the heat transfer capability of air is low, the role it can play is extremely limited. PCMs are still the main cold source of the system and the final destination of most heat.

Table 2
Sensitivity analysis of the convection heat transfer coefficient h.

Convection heat transfer coefficient h ($W/(m^2\cdot K)$)	Temperature of antenna driver (°C)	Temperature of MCU (°C)	Temperature of communication (°C)
20	112.31	90.05	90.14
40	112.35	90.09	90.18
60	112.37	90.11	90.21
80	112.39	90.13	90.22
100	112.40	90.14	90.24

2.3. Governing equation of each node

For a specific node, the heat accumulation of the node is equal to the sum of the heat input from neighboring nodes and the heat generated by itself. The equation of energy conservation for node i can be expressed as:

$$\sum_{j=1}^{m}\frac{T_j^t - T_i^t}{R_{ij}} + Q_i = \rho_i c_i V_i \frac{\left(T_i^{t+1} - T_i^t\right)}{\Delta t} \tag{1}$$

In this equation, the first term represents heat diffusion, meaning the heat input into node i from m neighbor nodes; the second term represents the heat source; and the third term represents heat accumulation.

The explicit finite difference scheme for transient heat conduction can be expressed as:

$$T_i^{t+1} = \frac{\Delta t}{\rho_i c_i V_i}\sum_{j=1}^{m}\frac{T_j^t}{R_{ij}} + \frac{Q_i \Delta t}{\rho_i c_i V_i} + \left(1 - \frac{\Delta t}{\rho_i c_i V_i}\sum_{j=1}^{m}\frac{1}{R_{ij}}\right)T_i^t \tag{2}$$

The temperature of nodes at moment $t+1$ can be determined through the temperature distribution at moment t. Therefore, the temperature trend can be continuously deduced from the initial temperature field to a certain moment. Based on numerical theory, the temperature at the next moment needs to be positively correlated with the current temperature to avoid numerical oscillation. The stability criterion for the explicit finite difference scheme is:

$$1 - \frac{\Delta t}{\rho_i c_i V_i}\sum_{j=1}^{m}\frac{1}{R_{ij}} \geq 0 \tag{3}$$

Eq. (3) can be further transformed as follows [34]:

$$\Delta t \leq \frac{\rho_i c_i V_i}{\sum_{j=1}^{m}\frac{1}{R_{ij}}} \tag{4}$$

The time step Δt is related to the thermal capacity and resistance. To ensure convergence of the scheme, the time step needs to be limited to a certain range. Moreover, the key parameters, such as the thermal resistance between nodes, the latent heat of PCMs, and the boundary conditions, need to be described by additional equations. For neighboring nodes with flat contact surfaces, the thermal resistance can be expressed as:

$$R_{ij} = \frac{l_i}{2\lambda_i S_{ij}} + \frac{l_j}{2\lambda_j S_{ij}} \tag{5}$$

For nodes with cylindrical contact surfaces, such as the inner and outer walls of a vacuum flask, the thermal resistance can be expressed as:

$$R_{ij} = \frac{\ln\left[\left(r_i^{in} + r_i^{out}\right)/2r_i^{in}\right]}{2\pi\lambda_i l} + \frac{\ln\left[2r_i^{in}\Big/\left(r_j^{in} + r_j^{out}\right)\right]}{2\pi\lambda_j l} \tag{6}$$

Notably, $r_i^{in} = r_j^{out}$.

Unlike thermal conduction in solid structures, the heat transfer process of PCMs includes heat conduction and phase change. For solid–liquid PCMs, an interface occurs during melting or solidification. Heat exchanges in the form of latent heat, and the interface moves during phase change. However, rather than the exact location of the interface, only the amount of heat that PCMs can store is needed in the modeling. Therefore, the square equivalent heat capacity method is used after specifying the properties of the PCMs. Assuming that the volume fraction of the liquid PCMs is linearly distributed in the phase-change region, the equivalent heat capacity can be expressed as [35]:

Table 3
Heat dissipation of the heat source inside the logging tool.

Heat source	Power dissipation (W)	Heat source	Power dissipation (W)
Communication	2 × 2	Power amplifier	3 × 3
MCU	2	Driver	3
Antenna driver	24	Others in total	47
Preamplifier	1		
Total power dissipation			90

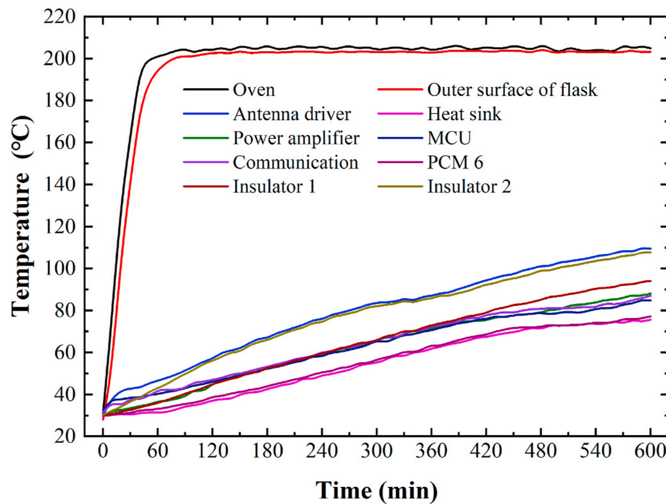

Fig. 5. Experimental temperature time series of the system.

$$c_{eff} = \begin{cases} c_s & (T < T_s) \\ \frac{1}{\rho_s}\left[\left(1 - \frac{T - T_s}{T_l - T_s}\right)\cdot\rho_s\cdot c_s + \frac{T - T_s}{T_l - T_s}\cdot\rho_l\cdot c_l\right] + \frac{L}{T_1 - T_s} & (T_s \le T \le T_l) \\ c_l & (T_l < T) \end{cases} \tag{7}$$

The outer surface of the vacuum flask, the mechanical joint, and the insulators are in direct convection heat transfer with the downhole environment, which can be expressed as:

$$q_i = hS_i(T_{\mathrm{envir}} - T_i) \tag{8}$$

The convection heat transfer coefficient of the outer surface of the flask in the oven is approximately 30∼40 W/(m^2·K) [14]. Table 2 shows the sensitivity analysis of the convection heat transfer coefficient. Changes in the convection heat transfer coefficients in this range of 20∼100 W/(m^2·K) have little effect on the actual temperature due to the good insulation of the flasks. Therefore, h = 35 W/(m^2·K) is set in our model. To verify the accuracy of the proposed model, the results are compared with the previous simulation.

3. Experiment setup

To verify the proposed model, a prototype is made, and a high-temperature experiment is conducted (see Fig. 4). Since the natural convection inside the PCM containers has little effect on the heat transfer process, this experiment is conducted horizontally [26]. Ceramic heating pads (40 × 40 × 2 mm) are used as substitutes for actual circuits with the same heating power and are attached to skeletons by TIMs. The heat dissipation of each heat source is shown in Table 3. Teflon tape is applied to fix the K-type thermocouples to the heat sources, PCMs, and other temperature measurement points. The skeleton with heat sources and thermocouples is loaded inside the flask and put into the oven (PTC1-40, Despatch). The temperature of the oven is set to 205 °C, and the heat sources are powered by DC power supplies (0–30 V/0–10 A, MS-3010D). The whole experiment lasts for 10 h, and the temperature is recorded with a data acquisition unit (0.2 % FS±, MIK-6000F).

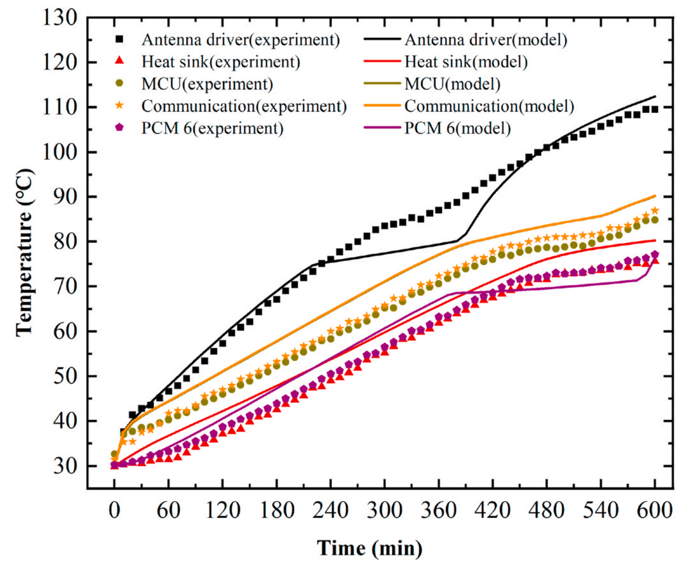

Fig. 6. Comparison of the results of the proposed model with the experiment.

4. Validation and discussion

4.1. Experimental results

Fig. 5 shows the results of the high-temperature experiment. The temperature inside the oven rises to 205 °C within 60 min, and that of the outer surface of the vacuum flask closely follows, which also rises to over 200 °C after 70 min. In contrast, the temperature of the circuits inside rises slowly. Affected by high-temperature heat leakage, the temperature near the opening side of the vacuum flask rapidly rises to 109.5 °C after 600 min, while other circuits are within 100 °C. In addition, before the shift in PCMs, the temperature rise slope of all circuits inside the vacuum flask remains constant. When the PCMs start melting and absorb heat, the temperature rise of the electronics is suppressed. The temperature rise rate of the MCU decreases from 5.7 °C/h to 2.0 °C/h before and during the phase change process. The circuit temperature starts to rise again at a relatively higher rate after the phase change.

4.2. Experiment validation and error analysis

To verify the accuracy and efficiency of the proposed model, the calculation results are compared with the experimental and simulation results. Fig. 6 shows the comparison with the experiment. The trends of both lines remain consistent, maintaining a slope of temperature growth close to constant outside the phase change process. Specifically, after 10 h of operation at an ambient temperature of 205 °C, the measured temperatures of the antenna driver, heat sink, MCU, communication and PCM 6 are 109.5 °C, 75.6 °C, 84.8 °C, 86.9 °C, and 77.1 °C, respectively. The corresponding calculated temperatures are 112.4 °C, 80.2 °C, 90.1 °C, 90.2 °C, and 76.3 °C, respectively. The maximum error between the calculation and experiment at 10 h is only 5.3 °C.

For the whole temperature rise process, the average relative error is approximately 6.5 %. In addition, the average absolute error between the experimental and model prediction results of all nodes is only 3.5 °C. The above results validate the accuracy of the model. As the error is less

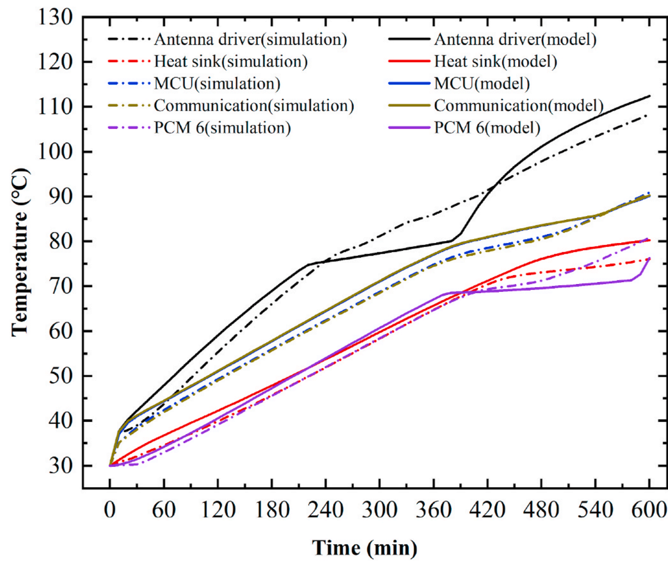

Fig. 7. Comparison of the results of the proposed model with numerical simulation.

than 10 °C, it is acceptable for the industrial application of a logging tool, which can be regarded as the engineering margin. The error mainly derives from the following aspects. On the one hand, the error comes from model assumptions. The proposed model assumes that all nodes are homothermic, and this assumption introduces an average error compared to the real situation. On the other hand, the experiment itself can introduce boundary error. Compared to the proposed model, the temperature of the oven is gradually heated from room temperature to 205 °C, while the model is set as directly convective heat transfer with the 205 °C oven environment. Furthermore, the model indicates a distinct melt region compared to the experiment. This discrepancy is attributed to the limited number of discrete nodes in the model. Without phase change, the temperature is primarily controlled by the sensible heat storage, and the temperature gradient within each node remains stable. However, during the phase change stage, the heat storage depends on the latent heat of PCM. The total PCMs are a non-isothermal body with different temperature gradient distribution. Therefore, there is some error in the phase transition interval, but the accuracy is enough throughout the temperature rise.

The accuracy of the model has been verified in different instruments and at different initial temperatures.

4.3. Comparison with simulation

Fig. 7 shows the comparison between the results of the proposed model and the numerical simulation [26]. Both temperature trends are close to each other, indicating that the proposed model is a good substitute for simulation. However, due to the small number of nodes and the neglect of the temperature distribution within nodes, the temperature curve during phase change is relatively stiff. Therefore, the error in the phase change interval is relatively large, with a maximum absolute error of approximately 7.7 °C.

Table 4 shows that the average absolute error between the simulation and experiment is 2.2 °C, with an average relative error of 4.0 %. In contrast, the accuracy of the model is slightly worse than that of the numerical simulation but still within the acceptable range. Specifically, the average absolute error between the predicted and experimental temperatures is 3.5 °C, and the average relative error is 6.5 %. The reason is that in the numerical simulation, 3175844 nodes are generated, so the temperature field can be presented with more complete details. In contrast, the proposed model has only 21 nodes, and the temperature jump between nodes is relatively larger. Only the temperature of each node at different moments can be obtained. With fewer nodes, the proposed model is much more efficient than numerical simulation. It takes only 0.8 s to obtain the results (CPU: i5-4590, memory: 32 G), while 50631 s is needed for numerical simulation. This shows that the proposed model can effectively balance the accuracy and real-time calculation efficiency. Therefore, the model can meet the

Table 4
Accuracy and efficiency analysis of the proposed model.

Method	Average absolute error compares with experiment (°C)	Average relative error compares with experiment (%)	Number of nodes	Calculation time (s)
Numerical simulation	2.2	4.0	3175844	50631
Proposed model	3.5	6.5	21	0.8

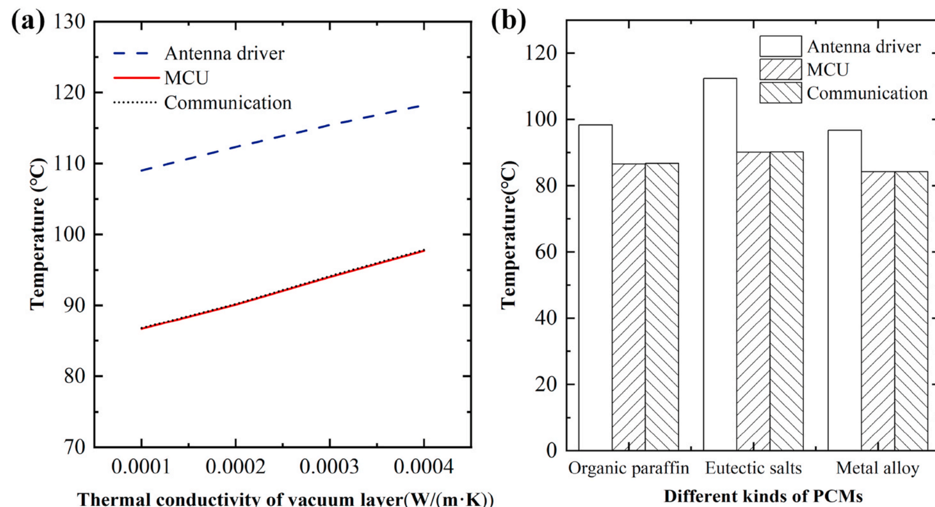

Fig. 8. Sensitivity analysis of different thermal properties:(a) different thermal conductivity of the vacuum layer; (b) different kinds of PCMs.

Table 5
Thermal properties of different PCMs.

Name	Eutectic salts [19]	Metal alloy [32]	Organic paraffin
Melting point (°C)	61.1	78.7	70
Latent heat (kJ/kg)	190.4	33.04	230
Thermal conductivity (W/(m·K))	0.50	18.8	0.2
Density (kg/m^3)	1485	9580	770
Specific heat (J/(kg·K)	1930	146	2000

requirements for real-time prediction of the temperature trend.

4.4. Sensitivity analysis

Fig. 8(a) and (b) is focused on the temperature of the key electronics of the logging tool at the end of the time. Fig. 8(a) depicts the influence of different thermal conductivity of the vacuum layer. The x-axis is the thermal conductivity (0.0001–0.0004 W/(m·K)), and the y-axis is the temperature of electronics at 600 min. Since the thermal shield effect is enhanced with lower thermal conductivity, the temperature of electronics is accordingly suppressed. The overall change demonstrates a linear trend, with the variation trends among different electronic components remaining remarkably consistent. When the thermal conductivity decreases from 0.0004 W/(m·K) to 0.0001 W/(m·K), the temperature of the antenna driver drops from 118.24 °C to 108.99 °C. The temperature-thermal conductivity slope is about 3×10^4 °C/(W/(m·K)).

As the main heat storage pool of the thermal management system, PCMs are critical for the temperature control of the heat sources. Fig. 8(b) displays the temperature of the electronics at the end of the time using three different kinds of PCMs, organic paraffin, eutectic salts and metal alloy. Table 5 shows the thermal properties of each PCM. The metal alloy demonstrates the optimal temperature control effect than another two materials. The average temperature is lowered by ~2 °C and ~6 °C compared with organic paraffin and eutectic salts, respectively.

5. Conclusion

A transient heat transfer model for predicting the temperature of logging tools in real time is developed. Its performance is examined by comparison with experimental and numerical simulation results. The average relative error of the temperature between the model and experiment is 6.5 %, and the average absolute error is 3.5 °C. This result firmly validates the accuracy of the model. Compared with the numerical simulation, the accuracy of the predicted temperature is only 1.3 °C worse, but the calculation time is reduced by 6×10^4 times; that is, the efficiency is greatly improved. The proposed model can be used to predict the temperature of downhole electronics under different working conditions.

CRediT authorship contribution statement

Fulong Wei: Writing – original draft, Visualization, Methodology, Investigation. **Wei Lan:** Methodology, Investigation. **Chao Deng:** Methodology, Investigation, Conceptualization. **Jiale Peng:** Visualization, Methodology, Investigation. **Xiaobing Luo:** Supervision, Resources, Project administration, Funding acquisition.

Declaration of competing interest

The authors declare that they have no known competing financial interests or personal relationships that could have appeared to influence the work reported in this paper.

Data availability

Data will be made available on request.

Acknowledgements

This research was supported by the Open Fund Science and Technology on Thermal Energy and Power Laboratory (No. TPL2022B02).

References

[1] C. Xu, W. Zou, Y. Yang, Y. Duan, Y. Shen, B. Luo, C. Ni, X. Fu, J. Zhang, Status and prospects of deep oil and gas resources exploration and development onshore China, J. Nat. Gas Sci. Eng. 3 (2018) 11–24, https://doi.org/10.1016/j.jnggs.2018.03.004.
[2] D. Xiao, Y. Hu, Y. Meng, G. Li, T. Wang, W. Chen, Research on wellbore temperature control and heat extraction methods while drilling in high-temperature wells, J. Pet. Sci. Eng. 209 (2022) 109814, https://doi.org/10.1016/j.petrol.2021.109814.
[3] A. Shadravan, M. Amani, Hpht 101 - what Every engineer or geoscientist should know about high pressure high temperature wells, SPE Kuwait International Petroleum Conference and Exhibition, Kuwait City, Kuwait (2012), https://doi.org/10.2118/163376-MS.
[4] C. Zeeden, A. Ulfers, S. Pierdominici, M.S. Abadi, M. Vinnepand, T. Grelle, K. Hesse, K. Leu, T. Wonik, Downhole logging data for time series analysis and cyclostratigraphy, Earth Sci. Rev. 241 (2023) 104436, https://doi.org/10.1016/j.earscirev.2023.104436.
[5] J. Watson, G. Castro, A review of high-temperature electronics technology and applications, J. Mater. Sci. Mater. Electron. 26 (2015) 9226–9235, https://doi.org/10.1007/s10854-015-3459-4.
[6] B. Holbein, J. Isele, Cooling systems for borehole tools, Journal of Geological Resource and Engineering (2013) 55–60, https://doi.org/10.17265/2328-2193/2013.01.007.
[7] S. Verma, Q. Elias, Thermal Management of Electronics Used in Downhole Tools, SPE Annual Technical Conference and Exhibition, San Antonio, Texas, USA, 2012, https://doi.org/10.2118/159737-MS.
[8] Q. Tao, M. Wei, H. Chen, A. Deng, Y. He, Thermal management system of vapor compression for downhole instrument, J. Therm. Sci. Eng. Appl. (2023), https://doi.org/10.1115/1.4062555.
[9] W. Gao, K. Liu, X. Dou, S. Tang, L. Zhang, Numerical investigation on cooling effect in the circuit cabin of active cooling system of measurement-while-drilling instrument based on split-Stirling refrigerator, Case Stud. Therm. Eng. 28 (2021) 101621, https://doi.org/10.1016/j.csite.2021.101621.
[10] W. Gao, K. Liu, X. Dou, L. Zhang, S. Tang, Numerical investigation on heat transfer rate from the outside environment into the electronic compartment of the measurement-while-drilling tools, Heat Transf 50 (2021) 5835–5852, https://doi.org/10.1002/htj.22151.
[11] A. Sinha, Y. Joshi, Application of thermoelectric-adsorption cooler for harsh environment electronics under varying heat load, J. Therm. Sci. Eng. Appl. 2 (2010), https://doi.org/10.1115/1.4002590.
[12] A. Stefánsson, R. Duerholt, J. Schroder, J. Macpherson, C. Hohl, T. Kruspe, T. Eriksen, A 300 Degree Celsius Directional Drilling System, IADC/SPE Drilling Conference and Exhibition, Fort Worth, Texas, USA, 2018, https://doi.org/10.2118/189677-MS.
[13] R. Weerasinghe, T. Hughes, Analysis of thermal performance of geophonic downhole measuring tools; a numerical and experimental investigation, Appl. Therm. Eng. 137 (2018) 504–512, https://doi.org/10.1016/j.applthermaleng.2018.03.090.
[14] S. Soprani, J.H.K. Haertel, B.S. Lazarov, O. Sigmund, K. Engelbrecht, A design approach for integrating thermoelectric devices using topology optimization, Appl. Energy 176 (2016) 49–64, https://doi.org/10.1016/j.apenergy.2016.05.024.
[15] W. Gao, K. Liu, Y. Su, L. Sheng, C. Cao, X. Dou, L. Zhang, Active Cooling Method for Downhole Systems in High Temperature Environment, SPE Western Regional Meeting, San Jose, California, USA, 2019, https://doi.org/10.2118/195353-MS.
[16] S. Soprani, Active Cooling of a Down Hole Well Tractor, Technical University of Denmark, 2016.
[17] Y. Lv, W. Chu, Q. Wang, Thermal management systems for electronics using in deep downhole environment: a review, Int. Commun. Heat Mass Tran. 139 (2022) 106450, https://doi.org/10.1016/j.icheatmasstransfer.2022.106450.
[18] J. He, Q. Wang, J. Wu, Y. Zhang, W. Chu, Hybrid thermal management strategy with PCM and insulation materials for pulsed-power source controller in extreme oil-well thermal environment, Appl. Therm. Eng. 214 (2022) 118864, https://doi.org/10.1016/j.applthermaleng.2022.118864.
[19] B. Shang, Y. Ma, R. Hu, C. Yuan, J. Hu, X. Luo, Passive thermal management system for downhole electronics in harsh thermal environments, Appl. Therm. Eng. 118 (2017) 593–599, https://doi.org/10.1016/j.applthermaleng.2017.01.118.
[20] Y. Ma, B. Shang, R. Hu, X. Luo, Thermal Management of Downhole Electronics Cooling in Oil & Gas Well Logging at High Temperature, 2016 17th International Conference on Electronic Packaging Technology, ICEPT, 2016, pp. 623–627, https://doi.org/10.1109/ICEPT.2016.7583211.
[21] J. Peng, W. Lan, Y. Wang, Y. Ma, X. Luo, Thermal Management of the High-Power Electronics in High Temperature Downhole Environment, IEEE 22nd Electronics

Packaging Technology Conference (EPTC), IEEE, 2020, pp. 369–375, https://doi.org/10.1109/EPTC50525.2020.9315026.
[22] K. Zhang, A. Guliani, S. Ogrenci-Memik, G. Memik, K. Yoshii, R. Sankaran, P. Beckman, Machine learning-based temperature prediction for runtime thermal management across system components, IEEE Trans. Parallel Distr. Syst. (2016), https://doi.org/10.1109/TPDS.2017.2732951.
[23] S. Durgam, A. Bhosale, V. Bhosale, R. Deshpande, P. Sutar, S. Kamble, Temperature prediction of heat sources using machine learning techniques, Heat Transf 50 (2021) 7817–7838, https://doi.org/10.1002/htj.22255.
[24] Z. Xue, C. Zhang, Z. Li, J. Cheng, An on-site temperature prediction method for passive thermal management of high-temperature logging apparatus, Meas. Control 55 (2022) 1180–1189, https://doi.org/10.1177/00202940221076809.
[25] A.K. Coskun, T.S. Rosing, K.C. Gross, Utilizing predictors for efficient thermal management in multiprocessor SoCs, IEEE Trans. Comput. Aided Des. Integrated Circ. Syst. 28 (2009) 1503–1516, https://doi.org/10.1109/TCAD.2009.2026357.
[26] W. Lan, J. Zhang, J. Peng, Y. Ma, S. Zhou, X. Luo, Distributed thermal management system for downhole electronics at high temperature, Appl. Therm. Eng. 180 (2020) 115853, https://doi.org/10.1016/j.applthermaleng.2020.115853.
[27] J. Peng, W. Lan, F. Wei, C. Deng, B. Xie, X. Luo, A numerical model coupling multiple heat transfer modes to develop a passive thermal management system for logging tool, Appl. Therm. Eng. 223 (2023) 120011, https://doi.org/10.1016/j.applthermaleng.2023.120011.
[28] A. Sur, B. Kouchmeshky, R. Satti, Thermal modeling of a wireline tool for ultra-high temperatures, in: 12th International Conference on Nanochannels, Microchannels, and Minichannels, 2014, https://doi.org/10.1115/FEDSM2014-21851. Chicago, Illinois, USA, 2014.
[29] A. Sinha, Y.K. Joshi, Downhole electronics cooling using a thermoelectric device and heat exchanger arrangement, J. Electron. Packag. 133 (2011), https://doi.org/10.1115/1.4005290.
[30] A. Lucherini, J.P. Hidalgo, J.L. Torero, C. Maluk, Numerical heat transfer model for swelling intumescent coatings during heating, Int. J. Therm. Sci. 184 (2023) 107922, https://doi.org/10.1016/j.ijthermalsci.2022.107922.
[31] A. Rhoads, D. Bacellar, C. Martin, R. Waser, M. Zaglio, Quasi Steady-State Modeling Approach for Low Computational Cost Design Optimization of Heat Exchangers for Phase Change Material (PCM) Thermal Batteries, International Refrigeration and Air Conditioning Conference, 2021.
[32] C. Deng, F. Wei, W. Lan, J. Peng, X. Luo, Experimental and numerical investigation of low melting point alloy for downhole electronics at high temperature, IEEE International Power Electronics and Application Conference and Exposition (PEAC) (2022), https://doi.org/10.1109/PEAC56338.2022.9959508.
[33] F. Wei, C. Deng, J. Peng, X. Luo, Thermal optimization of a logging tool used in high temperature downhole environment, IEEE International Power Electronics and Application Conference and Exposition (PEAC) (2022), https://doi.org/10.1109/PEAC56338.2022.9959495.
[34] W.J. Minkowycz, E.M. Sparrow, Handbook of Numerical Heat Transfer, second ed., Wiley, 2006.
[35] S.N. AL-Saadi, Z.J. Zhai, Modeling phase change materials embedded in building enclosure: a review, Renew. Sust. Energ. 21 (2013) 659–673, https://doi.org/10.1016/j.rser.2013.01.024.